NORDITA-96/68 P
SLAC-PUB-7342
hep-ph/9611278
September 2, 1997

Rapidity gaps in perturbative QCD

Stanley J. Brodsky[1]
Stanford Linear Accelerator
Stanford University, Stanford, California 94309, USA

Paul Hoyer[2] **and Lorenzo Magnea**[3]
NORDITA
Blegdamsvej 17, DK-2100 Copenhagen Ø, Denmark

Abstract

We analyze diffractive deep inelastic scattering within perturbative QCD by studying lepton scattering on a heavy quark target. Simple explicit expressions are derived in impact parameter space for the photon wave function and the scattering cross sections corresponding to single and double Coulomb gluon exchange. At limited momentum transfers to the target, the results agree with the general features of the "aligned jet model". The color-singlet exchange cross section receives a leading twist contribution only from the aligned jet region, where the transverse size of the photon wave function remains finite in the Bjorken scaling limit. In contrast to inclusive DIS, in diffractive events there is no leading twist contribution to σ_L/σ_T from the lowest order $(q\bar{q})$ photon Fock state, and the cross section for heavy quarks is power suppressed in the quark mass. There are also important contributions with large momentum transfer to the target, which corresponds to events having high transverse momentum production in both the projectile and target rapidity regions, separated by a rapidity gap.

[1]Work supported in part by Department of Energy contract DE-AC03-76SF00515 and DE-AC02-76ER03069.
[2]Work supported in part by the EU/TMR contract ERB FMRX-CT96-0008.
[3]On leave from Università di Torino, Italy

1 Introduction

The physics of rapidity gaps in deep inelastic lepton scattering (DIS) has been qualitatively described using the "aligned jet" model [1]. This model forms the basis for several QCD studies of diffractive DIS, where various assumptions have been made concerning the interaction with the target (Pomeron exchange [2], BFKL ladders [3], soft color fields [4]). In this paper we wish to test and clarify the physics of the aligned jet model by choosing a particularly simple target, which allows a full perturbative calculation. We believe that such an explicit (and straightforward) QCD calculation can serve to illustrate several points of principle, and help distinguish between the physics of the photon projectile and the target "diffractive structure function".

In the aligned jet model, the virtual photon breaks up into an asymmetric quark–antiquark pair. In the frame where the target is at rest, one of the two partons, say the quark, takes nearly all the photon energy ν, and forms the "current jet". The antiquark has then a finite energy of $\mathcal{O}(\Lambda_{QCD}/x)$, even in the scaling limit, $Q^2,\ \nu \to \infty$ with $x = x_{Bj} = Q^2/2m_N\nu$ fixed. The antiquark also has low transverse momentum $p_\perp = \mathcal{O}(\Lambda_{QCD})$ with respect to the photon direction, and scatters softly on the target. (Conversely, in the frame in which the target has infinite momentum, the antiquark is seen as a quark emerging from the target with momentum fraction x, and the soft scattering probability corresponds to the structure function.)

Since the antiquark momentum is proportional to $1/x$, it reaches quite high values in the small x range accessible at Hera. Thus, in analogy to hadron scattering, also the antiquark scattering is expected to develop a diffractive (color–singlet exchange) part, resulting in a "rapidity gap" between the antiquark and target.

The soft target scattering cannot be calculated in perturbation theory. In inclusive DIS, one relies on the QCD factorization theorem to separate the hard and soft momenta in the process. For diffractive DIS, however, there is no analogous proof of the separation of hard and soft subprocesses, so that the analysis is more model dependent and may provide new insights into the structure of hadrons and nuclei (see for example Ref. [5]).

Here we wish to study a very simple model for the target scattering by assuming that the target is a heavy quark [6]. This selects Coulomb gluon exchange as the dominant high energy interaction. We will consider both one and two–gluon exchange contributions in order to model the inclusive and diffractive DIS, respectively. Our approach can be viewed in two ways:

(i) As a toy model, consistent with PQCD (in fact it is PQCD, as the process we consider is theoretically conceivable). Many of our results will be similar to calculations involving more sophisticated assumptions about the target scattering, for example in terms of BFKL gluon ladders [3]. We feel that it is useful nevertheless to explicitly demonstrate those features which follow just

from the photon structure through the aligned jet mechanism, by making the simplest possible assumption about the target scattering.

(ii) As the lowest order of a more complete calculation which also takes into account gluon radiation and scattering. As noted above, in the target rest frame the antiquark is seen as part of the photon wave function; similarly, the (high energy part of the) gluon ladder to the target is built from gluons radiated from the initial quark pair. It is thus not unreasonable to expect the nature (and mass) of the target itself to be rather immaterial once sufficiently many gluons are considered in the photon wave function.

At small x and, consequently, large longitudinal momenta $p_z \sim \mathcal{O}(\Lambda_{QCD}/x)$, the parton interaction times in the target (which are of $\mathcal{O}(1$ fm$)$) are short compared to their (Lorentz–dilated) lifetimes. Hence the scattering amplitude factorizes into a Fock state formation amplitude (the photon wave function) and a scattering amplitude for each Fock state [7, 8, 9]. Moreover, the scatterer can move only a negligible transverse distance $\sim Lp_\perp/p_z$ in a soft scattering on a target of length L. Hence the scattering amplitude is approximately diagonal in impact parameter space. We show explicitly how these features arise in the PQCD amplitude for one and two gluon exchange at leading order in $1/x$. These features, which follow from general quantum mechanical principles, must be present to arbitrary orders in perturbation theory, providing an important conceptual and technical simplification of higher order calculations.

Since hadronization is an inherently non–perturbative phenomenon, it is not possible to prove that the rapidity gap between the target and diffractive scatterer is maintained in the evolution to the hadronic final state. Nevertheless, one can take a step in this direction by calculating the distribution of soft gluon radiation. This is analogous to the PQCD "proof" of the string effect in $e^+e^- \to q\bar{q}g \to$ hadrons [11]. From the structure of the photon wave function we verify that soft gluon radiation is indeed dominantly emitted in the rapidity region between the quark and the antiquark. We expect this feature to survive a scattering with color–singlet exchange, leaving a rapidity gap between hadrons in the photon and target fragmentation regions.

An immediate consequence of our analysis is that the dependence of the single–gluon exchange cross section on the photon energy ν dominates the multi–gluon exchange contribution by a factor of $\mathcal{O}(\log \nu)$, a feature that appears also in QED [12]. This logarithm is due to scattering at large impact parameters, which for a color–singlet target will saturate at impact parameters of the order of the target radius.

Our model also shows that there are important contributions to hard diffractive scattering from small impact parameters of $\mathcal{O}(1/Q)$. This should show up in ep scattering as events where both the projectile and the target fragment into large transverse momentum particles, with a rapidity gap between the projectile and target fragments.

The purpose of this paper is to present a self–contained perturbative model of diffractive DIS which bypasses the uncertainties due to Pomeron physics. With this in mind, we shall be rather explicit and assume no methods beyond the standard arsenal of perturbative QCD.

2 Scattering amplitudes on a massive target

In this section we will state the kinematic properties of our model, and present the calculation of the relevant amplitudes. We shall be concerned with the QCD amplitude for

$$\gamma^*(q) + t(m_t) \to q(p_1) + \bar{q}(p_2) + t(m_t) \quad , \tag{1}$$

where we take the target t to be a heavy quark of mass m_t. We shall calculate the process (1) in the small–x limit[1], at leading order in PQCD, and study both inclusive and diffractive DIS, the latter being defined by the requirement that the $q\bar{q}$ pair be in a color–singlet state after the scattering. In both cases, we demonstrate how the amplitude factorizes into the photon wave function (as derived in the Appendix) and the $q\bar{q}$ scattering amplitude.

The calculation is greatly simplified by assuming a large target mass m_t, which implies Coulomb gluon exchange and negligible energy transfer. The large target mass limit is thus a natural laboratory for perturbative studies of DIS and for the emergence of rapidity gaps. Since, as we shall see, much of the physics is encoded in the photon wave function, there is reason to hope that many features of the process will be target–independent and generally applicable to the physical case of a color–singlet, finite mass target.

The space–time picture we have in mind, depicted in Fig. 1 for double–gluon exchange, is thus the following. A high energy photon of energy ν and virtuality Q^2 fluctuates into a $q\bar{q}$ pair a long time ($\mathcal{O}(\nu/Q^2)$) before reaching the target. The pair subsequently interacts with the massive target via single or multiple Coulomb gluon exchange, with a limited total momentum transfer $\mathbf{K}$. For a diffractive process we require the pair to emerge from the scattering in a color–singlet state, so that a rapidity gap between the pair and the target can be formed.

We will work in the target rest frame in which the virtual photon is moving along the positive z axis, $q = (\nu, \mathbf{0}_\perp, \sqrt{\nu^2 + Q^2})$. The small value of Bjorken x implies that the photon is off–shell by an amount which is small compared with its energy,

$$q_z \simeq \nu + Q^2/2\nu \quad . \tag{2}$$

[1]We use the standard definition of $x = Q^2/2m_N\nu$, m_N being the nucleon mass. All our results will depend only on the combination $xm_N = Q^2/2\nu$ and are insensitive to the value of the (large) target mass m_t.

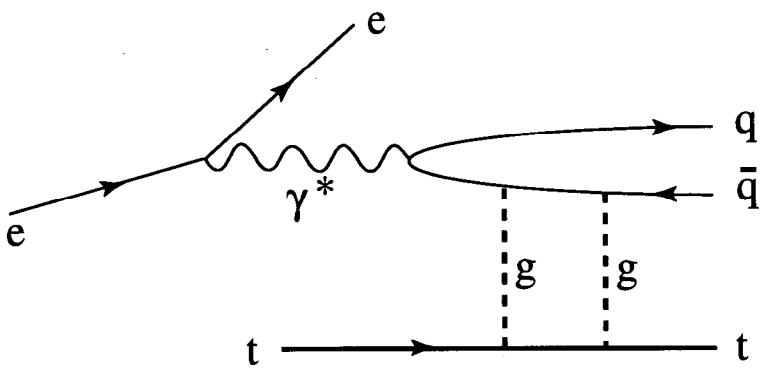

Figure 1: A diagram contributing to the process $e+t(m_t) \to q(p_1)+\bar{q}(p_2)+t(m_t)$ with double–gluon exchange.

We take all transverse momenta to be much smaller than the longitudinal ones. The 3–momenta of the quarks are parametrized as

$$\begin{aligned} \mathbf{p}_1 &= (\mathbf{p}_{1\perp}, zq_z) \ , \\ \mathbf{p}_2 &= (\mathbf{p}_{2\perp}, (1-z)q_z + K_z) \ , \end{aligned} \tag{3}$$

where $\mathbf{p}_{2\perp} = \mathbf{K}_\perp - \mathbf{p}_{1\perp}$. Energy transfer to the target is suppressed by powers of the target mass, so that energy conservation reads

$$\nu \simeq q_z + K_z + \frac{\mathbf{p}_{1\perp}^2 + m^2}{2z\nu} + \frac{\mathbf{p}_{2\perp}^2 + m^2}{2(1-z)\nu} \ . \tag{4}$$

This implies that the total longitudinal momentum K_z transferred to the target is small, of order Q^2/ν or $p_\perp^2/\nu$.

With these kinematic preliminaries in mind, we turn to the evaluation of the scattering amplitudes. In particular, using the standard decomposition of the total amplitude given in the Appendix, Eq. (60), we concentrate on the amplitude for process (1) with a virtual photon of definite polarization,

$$A(\lambda; \lambda_1, \lambda_2) = \boldsymbol{\epsilon}(\lambda) \cdot \mathbf{j}_h(\lambda_1, \lambda_2) \ , \tag{5}$$

where λ_1 and λ_2 are the helicities of the quark and the antiquark, respectively.

We first calculate the single Coulomb gluon exchange amplitude A_1, which in many respects is analogous to the two–gluon (color–singlet exchange) amplitude A_2. In particular, both amplitudes will turn out to factorize in impact parameter space into a product of the photon wave function (*cf* Appendix) and the $q\bar{q}$ scattering amplitude.

2.1 One–gluon exchange

The scattering amplitude is the sum of the two diagrams given in Fig. 2. Consider for example the first diagram, in which the Coulomb gluon is attached to the antiquark. In the limit of large mass m_t the target contributes only a factor $2m_t$ times the color factor $(T^a)_{CD}$. The fermion propagator in the upper vertex may be split into forward and backward propagating parts using the identity

$$\frac{\not{p}+m}{p^2-m^2+i\epsilon} = \frac{1}{2E}\left[\frac{E\gamma^0-\mathbf{p}\cdot\boldsymbol{\gamma}+m}{p^0-E+i\epsilon}+\frac{E\gamma^0+\mathbf{p}\cdot\boldsymbol{\gamma}-m}{p^0+E-i\epsilon}\right] \quad , \tag{6}$$

where $E=\sqrt{\mathbf{p}+m^2}$. This procedure splits the covariant diagram into different time orderings of the vertices, reproducing the results of time–ordered and light–cone perturbation theory. In the DIS limit, the fermion energies are $\gtrsim \mathcal{O}((\mathbf{p}_\perp^2+m^2)2\nu/Q^2)$, hence for small x we may neglect the backward scattering term in Eq. (6), and the denominator simplifies to

$$2E(p_0-E) \simeq -\frac{\mathbf{p}_{1\perp}^2+\varepsilon^2}{z} \tag{7}$$

where

$$\varepsilon^2 = m^2+z(1-z)Q^2 \quad . \tag{8}$$

The amplitude for Fig. 2a is then

$$\begin{aligned} A_1^{(1)}(\mathbf{p}_{1\perp},\mathbf{K}_\perp) &= ee_q g^2\,(T^a)_{AB}\,(T_a)_{CD}\,\frac{2m_t z}{\mathbf{K}^2(\mathbf{p}_{1\perp}^2+\varepsilon^2)} \\ &\times \sum_\beta [\bar{u}_{\lambda_1}(p_1)\boldsymbol{\varepsilon}(\lambda)\cdot\boldsymbol{\gamma}v_\beta(p_2-K)\;\bar{v}_\beta(p_2-K)\gamma_0 v_{\lambda_2}(p_2)] \quad . \end{aligned} \tag{9}$$

Using the explicit expressions for the spinors given in the Appendix, we have in the high energy limit

$$\bar{v}_\beta(p_2-K)\gamma_0 v_{\lambda_2}(p_2) = 2(1-z)\nu\delta_{\beta,\lambda_2} \quad . \tag{10}$$

The second diagram is treated similarly, giving

$$\begin{aligned} A_1^{(1)}(\mathbf{p}_{1\perp},\mathbf{K}_\perp) &= ee_q g^2\,(T^a)_{AB}\,(T_a)_{CD}\,\frac{4m_t\nu z(1-z)}{\mathbf{K}^2(\mathbf{p}_{1\perp}^2+\varepsilon^2)} \\ &\times \bar{u}_{\lambda_1}(p_1)\boldsymbol{\varepsilon}(\lambda)\cdot\boldsymbol{\gamma}v_{\lambda_2}(p_2-K) \quad , \\ A_1^{(2)}(\mathbf{p}_{1\perp},\mathbf{K}_\perp) &= -\,ee_q g^2\,(T^a)_{AB}\,(T_a)_{CD}\,\frac{4m_t\nu z(1-z)}{\mathbf{K}^2(\mathbf{p}_{2\perp}^2+\varepsilon^2)} \\ &\times \bar{u}_{\lambda_1}(p_1-K)\boldsymbol{\varepsilon}(\lambda)\cdot\boldsymbol{\gamma}v_{\lambda_2}(p_2) \quad . \end{aligned} \tag{11}$$

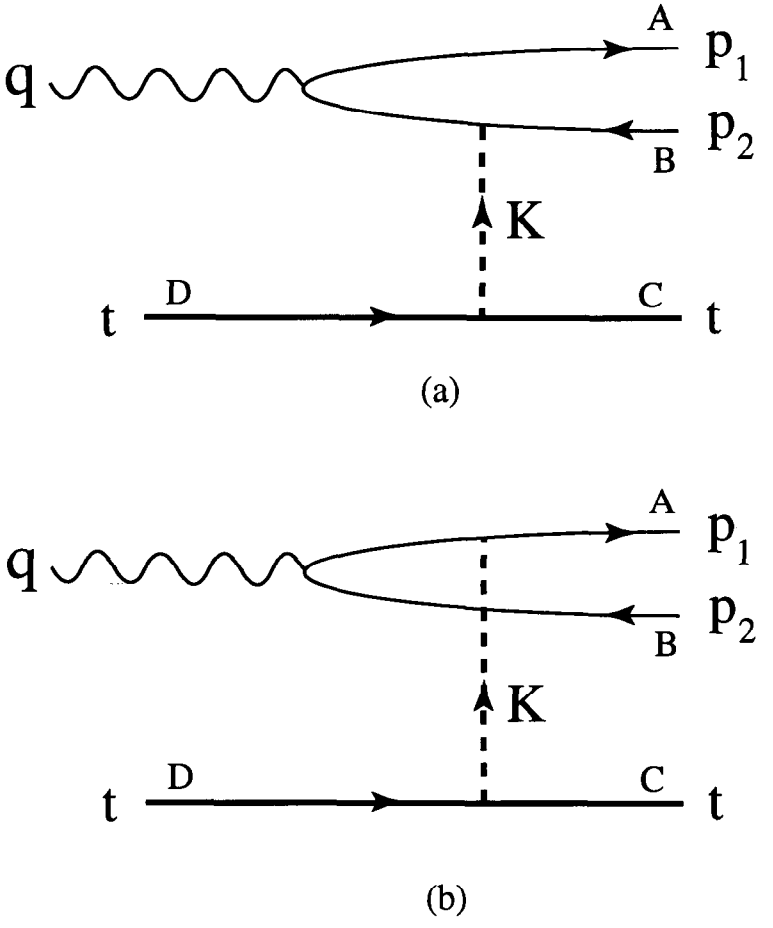

Figure 2: Single–gluon exchange diagrams contributing to inclusive deep inelastic scattering on a heavy quark target.

The close relationship between these amplitudes and the photon wave function given in the Appendix, Eq. (73), is already apparent. Fourier transforming to transverse distance space $\mathbf{r}_\perp$ between the quarks, by defining

$$A(\mathbf{r}_\perp, \mathbf{K}_\perp) = \int \frac{d^2\mathbf{p}_{1\perp}}{(2\pi)^2} A(\mathbf{p}_\perp, \mathbf{K}_\perp) \exp(i\mathbf{r}_\perp \cdot \mathbf{p}_{1\perp}) \quad , \tag{12}$$

we find consequently that the one–gluon exchange amplitude

$$A_1(\mathbf{r}_\perp, \mathbf{K}_\perp) = ig^2 2m_t (T^a)_{AB} \; (T_a)_{CD} W_1(\mathbf{r}_\perp, \mathbf{K}_\perp) V_\lambda^{\lambda_1,\lambda_2}(z, \mathbf{r}_\perp) \quad , \tag{13}$$

is proportional to the photon wave function $V_\lambda^{\lambda_1,\lambda_2}(z, \mathbf{r}_\perp)$ of Eq. (82). The eikonal factor

$$W_1(\mathbf{r}_\perp, \mathbf{K}_\perp) = \frac{1 - \exp(i\mathbf{r}_\perp \cdot \mathbf{K}_\perp)}{\mathbf{K}_\perp^2} \tag{14}$$

is independent of the photon helicity λ and of the quark helicities λ_1, λ_2. Since all dependence on the momentum transfer $\mathbf{K}_\perp$ to the target is in W_1, we may make a further transformation to target impact parameter ($\mathbf{R}_\perp$) space by defining

$$\begin{aligned} W_1(\mathbf{r}_\perp, \mathbf{R}_\perp) &= \int \frac{d^2\mathbf{K}_\perp}{(2\pi)^2} W_1(\mathbf{r}_\perp, \mathbf{K}_\perp) \exp(i\mathbf{R}_\perp \cdot \mathbf{K}_\perp) \\ &= \frac{1}{2\pi} \lim_{\epsilon \to 0} [K_0(|\mathbf{R}_\perp|\epsilon) - K_0(|\mathbf{R}_\perp + \mathbf{r}_\perp|\epsilon)] \\ &= \frac{1}{2\pi} \log\left(\frac{|\mathbf{R}_\perp + \mathbf{r}_\perp|}{|\mathbf{R}_\perp|}\right) \end{aligned} \tag{15}$$

The physical interpretation of our result, Eq. (13), is straightforward. The $q\bar{q}$ pair, which is in a color–singlet state before the scattering, forms a color dipole of size $\mathbf{r}_\perp$. This dipole cannot be detected by a gluon with $|\mathbf{K}_\perp| \lesssim 1/|\mathbf{r}_\perp|$, in which case the two diagrams tend to cancel. Thus in Eq. (15), $W_1 \propto |\mathbf{r}_\perp|/|\mathbf{R}_\perp|$ when this ratio is small. In particular, the infinite Coulomb phases associated with the quark and the antiquark cancel, and the eikonal factor is their finite remainder. In QED this factor would simply exponentiate upon adding extra virtual Coulomb photons. In non–abelian QCD the situation is complicated by color dynamics. The simple structure of Eq. (13) will, however, be preserved for more than one Coulomb gluon, in the color–singlet exchange channel.

2.2 Two–gluon exchange

Four diagrams contribute to the scattering amplitude via two–gluon exchange, corresponding to different attachments of the gluons to the quark and antiquark. The individual diagrams are infrared divergent, but their sum is finite because of the dipole cancellation discussed above. We regulate the infrared divergences by allowing only a finite time τ to elapse between the two gluon exchanges. With

a more realistic model for the target, τ would play the role of the target size, and we would expect $\tau \sim O(1/\Lambda_{QCD})$. Note that the true time interval between the two gluon exchanges is shorter than either the lifetime of the $q\bar{q}$ fluctuation or its subsequent hadronization time [7, 13]. Our infrared cutoff τ implies, as one can see by translating to time–ordered perturbation theory, an extra factor $1 - \exp(-\mathrm{i}K_{1z}\tau)$ in the amplitudes, where K_{1z} is the longitudinal momentum of one of the exchanged gluons. As we will see, the results are not sensitive to the specific value of the cutoff, which can be removed from the sum of the four diagrams.

Let us consider the diagram in Fig. 3, where the two gluons with momenta $\mathbf{K}_1$ and $\mathbf{K}_2$ ($\mathbf{K}_1 + \mathbf{K}_2 = \mathbf{K}$) interact with the antiquark line. Upon using the identity (6) on the fermion line between the gluon exchanges we encounter the energy denominator

$$\Delta E = -K_{1z} - \frac{1}{2z(1-z)\nu}\left[\varepsilon^2 + \mathbf{p}_{1\perp}^2 + z(\mathbf{K}_{1\perp}^2 - 2\mathbf{p}_{1\perp}\cdot\mathbf{K}_{1\perp})\right] \quad . \tag{16}$$

Since $K_{1z} \gtrsim \mathcal{O}(1/\tau)$ due to our cut–off, we have $\Delta E \simeq -K_{1z}$ at high energy ν.

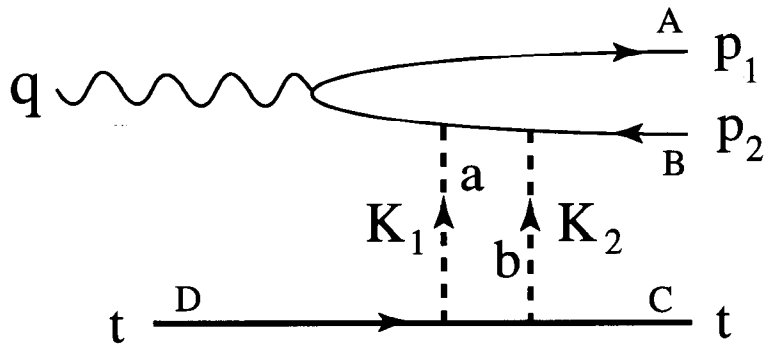

Figure 3: A two–gluon exchange diagram contributing to diffractive deep inelastic scattering on a heavy quark target.

It is legitimate to take the target mass limit $m_t \to \infty$ inside the loop integral, since the integral is ultraviolet convergent. Then the target contributes just an overall factor of $2m_t$ and a color coefficient, as for one–gluon exchange. The upper vertex also simplifies in the high energy limit, and finally we find

$$\begin{aligned} A_2^{(1,1)}(\mathbf{p}_{1\perp},\mathbf{K}_\perp) &= ee_q g^4\,(T^aT^b)_{AB}\,(T_bT_a)_{CD}\,\frac{4m_t\nu z(1-z)}{\mathbf{p}_{1\perp}^2+\varepsilon^2} \\ &\times\ \bar{u}_{\lambda_1}(p_1)\boldsymbol{\varepsilon}(\lambda)\cdot\boldsymbol{\gamma}v_{\lambda_2}(q-p_1)\int\frac{d^2\mathbf{K}_{1\perp}}{(2\pi)^2}J(K_{1\perp},K_{2\perp},\tau)\ , \end{aligned} \tag{17}$$

where J is the integral over the longitudinal component of the loop momentum. Using the fact that $K_z = K_{1z} + K_{2z}$ is negligible, the longitudinal momentum integral can be computed exactly,

$$\begin{aligned} J(a,b,\tau) &= \int_{-\infty}^{+\infty} \frac{dK_{1z}}{2\pi} \frac{1-\mathrm{e}^{-\mathrm{i}K_{1z}\tau}}{(K_{1z}^2+a^2)(K_{1z}^2+b^2)(K_{1z}-i\epsilon)} \\ &= \frac{\mathrm{i}}{2}\frac{1}{b^2-a^2}\left[\frac{1-\mathrm{e}^{-a\tau}}{a^2} - \frac{1-\mathrm{e}^{-b\tau}}{b^2}\right] \quad . \end{aligned} \tag{18}$$

Notice that for large values of τ this becomes simply

$$J(a,b,\tau) \sim \frac{\mathrm{i}}{2}\frac{1}{a^2 b^2} \quad , \tag{19}$$

independent of τ.

The other three diagrams can be treated in the same way. The longitudinal momentum dependence is encoded in the same integral, Eq. (18), for all of them. We find

$$\begin{aligned} A_2^{(1,2)}(\mathbf{p}_{1\perp},\mathbf{K}_\perp) &= -ee_q g^4\,(T^b T^a)_{AB}\,(T_b T_a)_{CD} \int \frac{d^2\mathbf{K}_{1\perp}}{(2\pi)^2} \frac{4m_t\nu z(1-z)}{(\mathbf{p}_{1\perp}-\mathbf{K}_{2\perp})^2+\varepsilon^2} \\ &\times\ \bar{u}_{\lambda_1}(p_1-K_2)\boldsymbol{\varepsilon}(\lambda)\cdot\boldsymbol{\gamma} v_{\lambda_2}(p_2-K_1) J(K_{1\perp},K_{2\perp},\tau) \quad , \\ A_2^{(2,1)}(\mathbf{p}_{1\perp},\mathbf{K}_\perp) &= -ee_q g^4\,(T^a T^b)_{AB}\,(T_b T_a)_{CD} \int \frac{d^2\mathbf{K}_{1\perp}}{(2\pi)^2} \frac{4m_t\nu z(1-z)}{(\mathbf{p}_{1\perp}-\mathbf{K}_{1\perp})^2+\varepsilon^2} \\ &\times\ \bar{u}_{\lambda_1}(p_1-K_1)\boldsymbol{\varepsilon}(\lambda)\cdot\boldsymbol{\gamma} v_{\lambda_2}(p_2-K_2) J(K_{1\perp},K_{2\perp},\tau) \quad , \\ A_2^{(2,2)}(\mathbf{p}_{1\perp},\mathbf{K}_\perp) &= ee_q g^4\,(T^b T^a)_{AB}\,(T_b T_a)_{CD} \frac{4m_t\nu z(1-z)}{\mathbf{p}_{2\perp}^2+\varepsilon^2} \\ &\times\ \bar{u}_{\lambda_1}(q-p_2)\boldsymbol{\varepsilon}(\lambda)\cdot\boldsymbol{\gamma} v_{\lambda_2}(p_2) \int \frac{d^2\mathbf{K}_{1\perp}}{(2\pi)^2} J(K_{1\perp},K_{2\perp},\tau) \quad . \end{aligned} \tag{20}$$

There are now two independent patterns of color flow, corresponding to singlet and octet exchange between the pair and the target. Since we are interested in the emergence of rapidity gaps, we project the amplitudes in Eqs. (17) and (20) onto singlet exchange by summing over the colors of the target quark. This is crucial to the present argument since only upon performing this projection do the four diagrams acquire the same weights (as in QED), and the eikonal factors in impact parameter space are similarly reconstructed. Upon summation over target color the color factors of all diagrams in fact reduce to that of the first one,

$$(T^a T^b)_{AB}(T_b T_a)_{CD}\,\delta^{CD} = \frac{1}{2} C_F \delta_{AB} \tag{21}$$

where $C_F = (N^2-1)/2N$.

The transverse momentum integrals associated with $A_2^{(1,2)}$ and with $A_2^{(2,1)}$ in Eq. (20) are more complicated than the others, since one more propagator depends on the loop momentum. This difficulty is however bypassed by once again

turning to coordinate space, as in Eq. (12). After the target color summation of Eq. (21) we find that the complete two–gluon color–singlet exchange amplitude,

$$A_2(\mathbf{r}_\perp, \mathbf{K}_\perp) = ig^4\, 2m_t \frac{1}{2} C_F \delta_{AB}\; W_2(\mathbf{r}_\perp, \mathbf{K}_\perp)\; V_\lambda^{\lambda_1,\lambda_2}(z, \mathbf{r}_\perp) \quad , \tag{22}$$

is, just like the single–gluon amplitude of Eq. (13), proportional to the photon wave function $V_\lambda^{\lambda_1,\lambda_2}(z, \mathbf{r}_\perp)$ of Eq. (82). The two–gluon eikonal factor is

$$W_2(\mathbf{r}_\perp, \mathbf{K}_\perp) = \int \frac{d^2\mathbf{K}_{1\perp}}{(2\pi)^2} J(K_{1\perp}, K_{2\perp}, \tau) \left(1 - e^{i\mathbf{r}_\perp \cdot \mathbf{K}_{1\perp}}\right) \left(1 - e^{i\mathbf{r}_\perp \cdot \mathbf{K}_{2\perp}}\right) \quad , \tag{23}$$

where $\mathbf{K}_2 = \mathbf{K} - \mathbf{K}_1$. The $\mathbf{K}_{1\perp}$ integral is now finite, due to the extra suppression for small $K_{1\perp}$ and $K_{2\perp}$ provided by the eikonal numerators. It is thus possible to let the cutoff $\tau \to \infty$, and use for J the simple expression given in Eq. (19). As a result we see that the two–gluon eikonal factor is a convolution of two one–gluon factors, Eq. (14), and can be written as

$$\begin{aligned} W_2(\mathbf{r}_\perp, \mathbf{K}_\perp) &= \frac{i}{2} \int \frac{d^2\mathbf{K}_{1\perp}}{(2\pi)^2} \frac{1 - e^{i\mathbf{r}_\perp \cdot \mathbf{K}_{1\perp}}}{K_{1\perp}^2} \int \frac{d^2\mathbf{K}_{2\perp}}{(2\pi)^2} \frac{1 - e^{i\mathbf{r}_\perp \cdot \mathbf{K}_{2\perp}}}{K_{2\perp}^2} \\ &\times (2\pi)^2 \delta^2(\mathbf{K}_\perp - \mathbf{K}_{1\perp} - \mathbf{K}_{2\perp}) \quad . \end{aligned} \tag{24}$$

Transforming $W_2(\mathbf{r}_\perp, \mathbf{K}_\perp)$ to $\mathbf{R}_\perp$-space as in Eq. (15) gives

$$\begin{aligned} W_2(\mathbf{r}_\perp, \mathbf{R}_\perp) &= \frac{i}{2} [W_1(\mathbf{r}_\perp, \mathbf{R}_\perp)]^2 \\ &= \frac{i}{8\pi^2} \left[\log\left(\frac{|\mathbf{R}_\perp + \mathbf{r}_\perp|}{|\mathbf{R}_\perp|}\right)\right]^2 \quad . \end{aligned} \tag{25}$$

The fact that the two–gluon eikonal factor W_2 is the square of the single gluon factor W_1 is a consequence of the conservation of the impact parameters $\mathbf{r}_\perp, \mathbf{R}_\perp$ during the scattering, and will clearly generalize to an arbitrary number of exchanges in the singlet channel. It has an important consequence for the energy dependence of the cross section, which was first noticed in QED by Bethe and Maximon [12]. The cross section for single–gluon exchange involves an integral which is logarithmically divergent at large impact parameters $\mathbf{R}_\perp$ to the target,

$$\int d^2\mathbf{R}_\perp |W_1|^2 \propto \int^{2\nu/Q^2} \frac{d^2\mathbf{R}_\perp}{\mathbf{R}_\perp^2} \quad . \tag{26}$$

This results in a cross section which grows logarithmically with the projectile energy. For two or more gluon exchanges the integral is on the other hand convergent at large $\mathbf{R}_\perp$, and no logarithm is generated.

3 Cross–sections

Our results for the one and two–gluon exchange amplitudes $\gamma^* t \to q\bar{q}t$ (5) can be summarized (see Eqs. (13) and (22)) as

$$A_n(\mathbf{r}_\perp, \mathbf{R}_\perp) = c_n \; m_t \; W_n(\mathbf{r}_\perp, \mathbf{R}_\perp) \; V(z, \mathbf{r}_\perp) \;\; , \tag{27}$$

where $\mathbf{r}_\perp$, $\mathbf{R}_\perp$ are the transverse distances between the produced quarks and between them and the target, respectively. The photon wave function $V(z, \mathbf{r}_\perp)$ is given in Eq. (82) and the eikonal factors $W_n(\mathbf{r}_\perp, \mathbf{R}_\perp)$ for $n = 1,\ 2$ gluon exchange in Eqs. (15) and (25), respectively. The coefficients c_n,

$$\begin{aligned} c_1 &= 2ig^2 (T^a)_{AB} (T_a)_{CD} \;\; , \\ c_2 &= ig^4 C_F \delta_{AB} \;\; , \end{aligned} \tag{28}$$

reflect the color structure.

The spin–averaged square of the full $et \to eq\bar{q}t$ amplitude T_n can be expanded as in Eq. (65),

$$\overline{|T_n|^2} = \frac{4e^4 e_q^2}{\pi^2} \frac{\nu^2 m_t^2}{y^2 Q^2} \, |c_n W_n(\mathbf{r}_\perp, \mathbf{R}_\perp)|^2 \; z(1-z) F(z, \mathbf{r}_\perp) \;\; , \tag{29}$$

with

$$\begin{aligned} F(z, \mathbf{r}_\perp) &= \tfrac{1}{2}[1 + (1-y)^2] \left\{ [1 - 2z(1-z)] \varepsilon^2 K_1^2(\varepsilon r_\perp) + m^2 K_0^2(\varepsilon r_\perp) \right\} \\ &+ 4(1-y)[z(1-z)]^2 Q^2 K_0^2(\varepsilon r_\perp) \\ &- 2(1-y)\cos(2\varphi) z(1-z) \varepsilon^2 K_1^2(\varepsilon r_\perp) \;\; , \end{aligned} \tag{30}$$

where we have used the explicit expression for the photon wave function derived in the Appendix (see also Ref. [9]). Here φ is the azimuthal angle between the lepton plane and the interquark separation $\mathbf{r}_\perp$.

The cross–section is given by

$$Q^2 \frac{d\sigma}{dQ^2 dx d\varphi} = \frac{1}{(4\pi)^8} \frac{4m_N}{m_t^2 \nu} \int \frac{dz}{z(1-z)} d^2\mathbf{K}_\perp d^2\mathbf{p}_{1\perp} \, \overline{|T|^2} \;\; , \tag{31}$$

where m_t is the target mass. We may thus define a "cross–section" in impact parameter space as

$$Q^4 \frac{d\sigma_n}{dQ^2 dx d\varphi d^2\mathbf{R}_\perp} = \frac{\alpha^2 e_q^2}{(2\pi)^4} \frac{Q^2}{xy^2} \int_0^{\frac{1}{2}} dz \int d^2\mathbf{r}_\perp \, |c_n W_n(\mathbf{r}_\perp, \mathbf{R}_\perp)|^2 \, F(z, \mathbf{r}_\perp), \tag{32}$$

whose integral over $\mathbf{R}_\perp$ gives the usual DIS cross section. In the Bjorken scaling limit (63) this cross–section should (at leading twist) be independent of Q^2.

In considering the properties of Eq. (32) it is important to distinguish the regions of large and small impact parameters $R_\perp$, corresponding to small and

large momentum transfer to the target, respectively. Most of the HERA data on rapidity gaps is selected for small momentum transfer, with the target (proton) diffracting into a low mass system [14]. Large momentum transfers implies particles or jets with large transverse momentum also at target rapidities. There is experimental evidence for this type of diffractive events as well [15].

3.1 Low momentum transfer to the target: $R_\perp \gg 1/m$

The Bessel functions $K_{0,1}(\varepsilon r_\perp)$ in Eq. (30) limit the size of the quark pair to $r_\perp^2 \lesssim \min\{1/m^2, 1/z(1-z)Q^2\}$. Hence for $R_\perp \gg 1/m$ we have also $R_\perp \gg r_\perp$, and the eikonal factors (15) and (25), integrated over the azimuthal angle φ_R between $\mathbf{R}_\perp$ and $\mathbf{r}_\perp$, are approximately

$$\int_0^{2\pi} d\varphi_R \, |W_n|^2 = a_n \left(\frac{r_\perp}{R_\perp}\right)^{2n} \quad , \tag{33}$$

where $a_1 = 1/4\pi$ and $a_2 = 3\pi/(4\pi)^4$. The integrals over $\mathbf{r}_\perp$ in Eq. (32) can then be done using

$$\int_0^\infty dr_\perp^2 \, r_\perp^{2n} K_j^2(\varepsilon r_\perp) = \frac{b_{jn}}{\varepsilon^{2n+2}} \quad , \tag{34}$$

where the b_{jn} ($j = 0, 1$; $n = 1, 2$) are numerical constants. Altogether the cross section becomes

$$\begin{aligned} Q^4 \frac{d\sigma_n}{dQ^2 dx d\varphi dR_\perp^2}\bigg|_{R_\perp \gg 1/m} &= \frac{\alpha^2 e_q^2}{4(2\pi)^3} \frac{Q^2}{xy^2} |c_n|^2 \frac{a_n}{R_\perp^{2n}} \\ \times \int_0^{\frac{1}{2}} \frac{dz}{\varepsilon^{2n+2}} &\Big\{ \tfrac{1}{2}[1 + (1-y)^2] \left[(1 - 2z(1-z))\varepsilon^2 b_{1n} + m^2 b_{0n} \right] \\ + \; 4(1-y)[z(1-z)]^2 Q^2 b_{0n} &- 2(1-y)\cos(2\varphi) z(1-z)\varepsilon^2 b_{1n} \Big\} \quad . \end{aligned} \tag{35}$$

There are two regions of the final z-integral in Eq. (35) that should be considered separately.

(a) $z = \mathcal{O}(m^2/Q^2)$, $r_\perp = \mathcal{O}(1/m)$.

This is the "aligned jet region" [1], relevant to the lowest order DIS process $\gamma^* q \to q$. In this region ε is finite ($\mathcal{O}(m)$), so the exponential suppression in the Bessel functions in Eq. (34) forces $r_\perp$ to be of order $1/m$. Thus in the scaling limit one of the quarks has a finite momentum, $z\nu \simeq m^2/2m_N x$, and the transverse size of the quark pair also remains finite. Only terms in the integrand of Eq. (35) that are of $\mathcal{O}(z^0)$ contribute. Hence the last two terms, which arise from photons with $\lambda = 0$ and from $\lambda = \pm 1$ interference, respectively, can be ignored, and the leading twist cross section is isotropic in azimuth. Since ε is finite, this region contributes both to the single and to the double–gluon exchange cross sections ($n = 1, 2$). This is as expected, since attaching several gluons to the quark pair does not change the scaling behavior of the cross section when the transverse size of the pair is fixed.

(b) $z = \mathcal{O}(\frac{1}{2})$, $r_\perp = \mathcal{O}(1/Q)$.

In this region both quarks take a finite fraction of the photon momentum, so that $\varepsilon = \mathcal{O}(Q)$, which in turn forces the transverse size of the pair to decrease with Q. The photon fragments thus typically have large transverse momentum. Since $\varepsilon \propto Q$, the contribution from this region to double–gluon color–singlet exchange ($n = 2$) is suppressed by a factor $1/Q^2$, *ie*, it is of higher twist. This is due to the compactness of the quark pair, which suppresses gluon attachment. In the case of single gluon exchange the suppression is compensated by the larger phase space available in z, compared to case (a). In the infinite momentum frame, the contribution of region (b) with $n = 1$ corresponds to the process $\gamma^* g \to q\bar{q}$ in inclusive DIS, which is suppressed only logarithmically by the running coupling $\alpha_s(Q^2)$.

We conclude that, for moderate momentum transfer to the target, the color–singlet ($n = 2$) cross section (35) gets a scaling contribution only from the aligned jet region (a). After the final z integration, we find

$$Q^4 \frac{d\sigma_2}{dQ^2 dx d\varphi dR_\perp^2}\bigg|_{R_\perp \gg 1/m} = \frac{\alpha^2 e_q^2}{4(2\pi)^3} \frac{|c_2|^2}{xy^2} \times \frac{a_2}{2R_\perp^4 m^2} \frac{1}{2}[1 + (1-y)^2]\,(2b_{12} + b_{02}) \quad . \quad (36)$$

Notice that, according to Eq. (36), the heavy quark diffractive cross–section decreases with the quark mass m as $1/m^2$. This is analogous to the suppression of diffractive production in the symmetric region (b) above. The size of a heavy quark pair is small, $r_\perp = \mathcal{O}(1/m)$, suppressing the coupling of multiple gluons. However, heavy quarks can be produced at leading power in the quark mass through higher Fock states of the photon, such as $q\bar{q}g$. The two–gluon exchange can then occur off the soft gluon in the Fock state, if it has a finite momentum and thus also a finite transverse size distribution in the scaling limit (see Section 4).

It is also interesting to compare our analysis with the perturbative QCD calculations[16] for diffractive vector meson leptoproduction: $\gamma^* p \to Vp$. In that case the leading contribution to the cross section arises from longitudinally–polarized photons and the symmetric regime $z = \mathcal{O}(\frac{1}{2})$, $r_\perp = \mathcal{O}(1/Q)$. Because of the color cancellations the exclusive diffractive cross section is suppressed by a factor $1/Q^4$ relative to the Bjorken–scaling rapidity gap rate.

3.2 Sum over target momentum transfers

In the remainder of this section we will focus on color–singlet exchange. Since the eikonal factor $W_2(\mathbf{r}_\perp, \mathbf{R}_\perp)$ according to Eq. (25) depends only on the ratio

$|\mathbf{R}_\perp + \mathbf{r}_\perp|/|\mathbf{R}_\perp|$, an integral over all impact pararameters $\mathbf{R}_\perp$ in the cross section (32) can be readily done. By dimensional analysis

$$\int d^2\mathbf{R}_\perp \, |W_2(\mathbf{r}_\perp, \mathbf{R}_\perp)|^2 = d_2 r_\perp^2 \quad , \tag{37}$$

where d_2 is a calculable numerical constant. When unconstrained, the typical value of $R_\perp$ in the cross section (32) is always of $\mathcal{O}(r_\perp)$. Note that the power of $r_\perp$ in Eq. (37) differs from that of Eq. (33) (valid for $R_\perp \gg r_\perp$). In terms of the constants b_{jn} of Eq. (34) we thus find the $\mathbf{R}_\perp$–integrated cross section to be

$$\begin{aligned} Q^4 \frac{d\sigma_2}{dQ^2 dx d\varphi} &= \frac{\pi\alpha^2 e_q^2}{(2\pi)^4} \frac{Q^2}{xy^2} |c_2|^2 d_2 \int_0^{\frac{1}{2}} \frac{dz}{\varepsilon^4} \\ &\times \left\{ \tfrac{1}{2}[1+(1-y)^2] \left[(1-2z(1-z))\varepsilon^2 b_{11} + m^2 b_{01} \right] \right. \\ &+ \left. 4(1-y)[z(1-z)]^2 Q^2 b_{01} - 2(1-y)\cos(2\varphi) z(1-z)\varepsilon^2 b_{11} \right\} \quad , \end{aligned} \tag{38}$$

In region (a) of the z integral in Eq. (38) ($z = \mathcal{O}(m^2/Q^2)$, *cf* Section 3.1), $r_\perp$ (and hence also $R_\perp$) is finite in the scaling limit. The scattering then dominantly proceeds via moderate momentum transfer $\mathcal{O}(1/R_\perp)$ to the target. On the other hand, for finite values of z in Eq. (38) the typical values of $R_\perp$ are of $\mathcal{O}(1/Q)$, implying large momentum transfers to the target. The corresponding inclusive DIS process is then $\gamma^* t \to q\bar{q}t$, where for a realistic target t would be a light quark (or gluon) constituent. Now the two–gluon exchange process is not suppressed since the typical hardness of the gluons is commensurate with the size of the $q\bar{q}$ dipole. This hard diffractive process (like its inclusive equivalent) is only suppressed by powers of the running coupling $\alpha_s(Q^2)$.

The z integration in Eq. (38) can readily be performed, and the leading twist contribution extracted. We find

$$\begin{aligned} Q^4 \frac{d\sigma_2}{dQ^2 dx d\varphi} &= \frac{\pi\alpha^2 e_q^2}{(2\pi)^4} \frac{|c_2|^2 d_2}{xy^2} \left\{ \frac{1}{2}[1+(1-y)^2] \left[b_{01} - b_{11} \left(1 - \log \frac{Q^2}{m^2} \right) \right] \right. \\ &+ \left. (1-y)\,(2b_{01} - b_{11}\cos(2\varphi)) \right\} \quad . \end{aligned} \tag{39}$$

Notice that for hard diffractive events the azimuthal distribution is not isotropic, and a logarithmic dependence on Q^2 is generated, since a much larger range in $p_\perp$ is now available.

3.3 Discussion

To summarize, there are two quite distinct kinematical regions contributing to the leading–twist color–singlet exchange cross section, Eq. (39). For small momentum transfers to the target, or equivalently for large impact parameter $R_\perp$,

our calculation provides a concrete realization of the aligned jet model [1]: asymmetric quark pairs with finite transverse size dominate in the scaling limit, with the scattering occurring off the slow quark. In this case the cross section is purely transverse and independent of azimuth. If, however, we allow for large momentum trasfers to the target, we find that the color–singlet cross section receives leading twist contributions from symmetric and narrow pairs. These contributions have a distinct azimuthal dependence and rise logarithmically with Q^2. They will appear as events with particles (or jets) of large transverse momentum in both the current and target fragmentation regions, which balance each other and are separated by a large rapidity gap. There is already experimental evidence for such events from ZEUS [15].

Our diffractive cross section (39) has no contribution corresponding to events with large transverse momentum jets only in the current fragmentation region, with low momentum transfer to the target. Such contributions should occur at higher orders in QCD, for $q\bar{q}g$ Fock states of the photon (see Section 4).

As we have seen, the low–x cross section is particularly simple when expressed in impact parameter space. Impact parameters are not directly measurable, since events are observed in momentum space. For integrated cross sections this is not an issue, as an integral over all impact parameters is equivalent to an integral over all transverse momenta. On the other hand, more differential predictions concerning, *eg*, the dependence of the cross section on the mass M^2 of the diffractive system, and on the size of the rapidity gap $\Delta\eta$, are less straightforward. At this stage we only make the following qualitative remarks.

The dependence of the diffractive cross section (32) on the mass M of the $(q\bar{q})$ system is usually parametrized through the variable[2]

$$\beta \equiv \frac{Q^2}{Q^2+M^2} = \frac{\varepsilon^2 - m^2}{\varepsilon^2 + |\mathbf{p}_{1\perp} - z\mathbf{K}_\perp|^2} \quad , \tag{40}$$

where $\varepsilon^2 = m^2 + z(1-z)Q^2$, as before. The rapidity gap η extends from the target (which is at rest and thus has zero rapidity) to the slow quark, and (for $z < 1/2$) is given by

$$\Delta\eta = \log\left(\frac{2z\nu}{m_{1\perp}}\right) \quad , \tag{41}$$

where $m_{1\perp} = \sqrt{p_{1\perp}^2 + m^2}$. Notice that we use a frame where the γ^* is moving along the z-axis.

We can estimate the average size of the rapidity gap in the various kinematical regions contributing to the cross section from the uncertainty relation corresponding to Eq. (12),

$$p_{1\perp} \simeq \frac{1}{r_\perp} \quad . \tag{42}$$

[2]In the framework of Pomeron exchange models, β is the fraction of Pomeron momentum carried by the struck quark.

In the aligned jet region we have (as discussed above) $\langle r_\perp \rangle \sim 1/m$, and hence $\langle p_{1\perp} \rangle \sim m$. Since in this region $z \sim m^2/Q^2$ the typical rapidity gap will be

$$\Delta\eta \sim \log\left(\frac{m}{m_N x}\right) \quad . \tag{43}$$

For large momentum transfer to the target, on the other hand, region (b) contributes to the cross section, so that $\langle r_\perp \rangle \sim 1/Q$, and consequently $\langle p_{1,\perp} \rangle \sim Q$. Furthermore, in this region $z \sim 1/2$, so that the size of the gap will now depend on Q. We get

$$\Delta\eta \sim \log\left(\frac{Q}{m_N x}\right) \quad . \tag{44}$$

The typical value of β remains finite in both regions, as it should. However we expect region (b) to give a relatively larger contribution at small values of β, since the diffractive system contains large $p_\perp$ jets. Furthermore it should be kept in mind that higher order contributions from gluon radiation will tend to increase the cross section at low β.

The estimates (43), (44) for the size of the rapidity gap are at the parton level. Hadronization may to some extent fill in the gap. In the next section we shall address this question by studying the angular distribution of soft gluon radiation.

4 Soft Gluon Radiation

In the case of color–singlet exchange one expects that hadrons will be produced mainly in the rapidity interval between the quarks, leaving a gap between the slower quark and the target (here at zero rapidity). While this hadronization pattern cannot be demonstrated using perturbative methods, it may be corroborated by studying the distribution of soft (but perturbative) gluons [10]. This is analogous to the successful description [11] of the "string effect" in e^+e^- annihilation.

Just as in the $q\bar{q}$ case above, we expect the gluon distribution in the final state to be largely determined by its distribution in the photon wave function. At lowest order, the $q\bar{q}g$ component of the photon is given by the two diagrams in Fig. 4. Using the prescription (71) and the identity (6) to select the dominant time ordering, we find

$$\begin{aligned} V(q\bar{q}g) &= i\frac{ee_q g T^a_{AB}}{\Delta E}\bar{u}(p_1)\left[\not{\epsilon}^*(k)\frac{1}{2E_{k1}}\frac{E_{k1}\gamma^0 - (\mathbf{k}+\mathbf{p}_1)\cdot\boldsymbol{\gamma} + m}{E_\gamma - E_2 - E_{k1} + i\epsilon}\boldsymbol{\epsilon}(q)\cdot\boldsymbol{\gamma}\right. \\ &- \left.\boldsymbol{\epsilon}(q)\cdot\boldsymbol{\gamma}\frac{1}{2E_{k2}}\frac{E_{k2}\gamma^0 - (\mathbf{k}+\mathbf{p}_2)\cdot\boldsymbol{\gamma} - m}{E_\gamma - E_1 - E_{k2} + i\epsilon}\not{\epsilon}^*(k)\right] v(p_2) \end{aligned} \tag{45}$$

where $E_\gamma = \sqrt{\mathbf{q}^2 - Q^2}$, $E_i = \sqrt{\mathbf{p}_i^2 + m^2}$, $E_{ki} = \sqrt{(\mathbf{k}+\mathbf{p}_i)^2 + m^2}$ and $\Delta E = E_\gamma - E_1 - E_2 - |\mathbf{k}| + i\epsilon$.

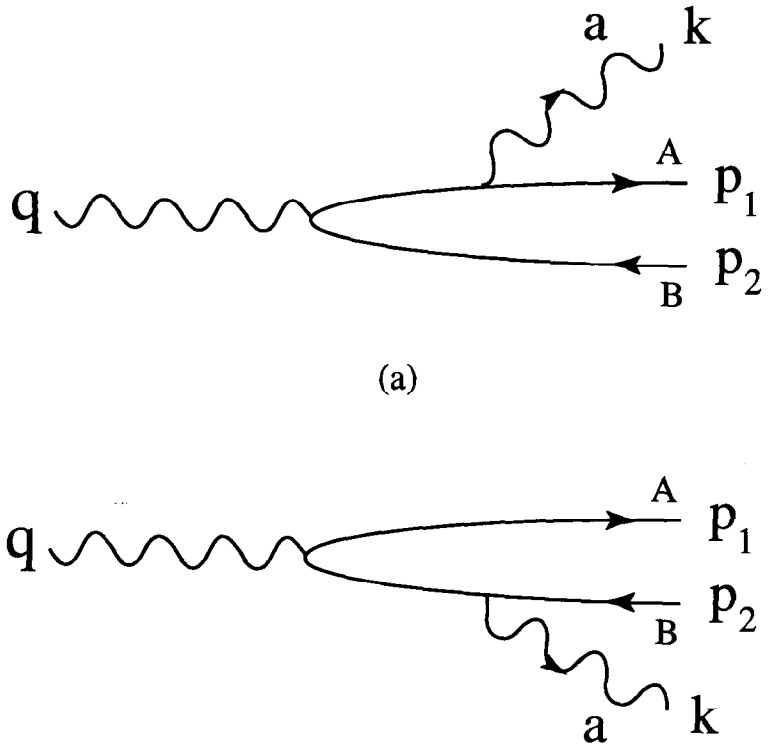

Figure 4: Lowest order diagrams describing the $q\bar{q}g$ Fock state of the photon.

In the soft gluon limit, $k_z \ll p_{1z}$, p_{2z} and $|\mathbf{k}_\perp| \ll |\mathbf{p}_{1\perp}|$, $|\mathbf{p}_{2\perp}|$, the $q\bar{q}g$ Fock state amplitude (45) factorizes into a product of the $q\bar{q}$ amplitude and a gluon emission factor,

$$V(q\bar{q}g) = V(q\bar{q})\, gT^a_{AB}\, \frac{1}{\Delta E}\, \varepsilon^*(k) \cdot \left(\frac{p_1}{E_1} - \frac{p_2}{E_2}\right) \tag{46}$$

with $V(q\bar{q})$ given by Eq. (73). The gluon angular distribution is thus governed by the factor

$$P(k) = \frac{1}{(\Delta E)^2} \sum_{\lambda_g} \left| \varepsilon^*_{\lambda_g}(k) \cdot \left(\frac{p_1}{E_1} - \frac{p_2}{E_2}\right)\right|^2 \quad , \tag{47}$$

where the sum is over the two transverse polarizations available to the gluon.

To evaluate Eq. (47), let us for clarity choose the frame so that the gluon is emitted in, say, the $x-z$ plane, *ie*, $k^\mu = (k, k\sin\theta, 0, k\cos\theta)$. Within the approximations discussed in Section 2, we find that the sum over polarizations yields

$$\sum_{\lambda_g} \left| \varepsilon^*_{\lambda_g}(k) \cdot \left(\frac{p_1}{E_1} - \frac{p_2}{E_2}\right)\right|^2 = \frac{\cos^2\theta (p^x_\perp)^2 + (p^y_\perp)^2}{\nu^2 z^2 (1-z)^2} \quad , \tag{48}$$

while the energy denominator is given by

$$-\Delta E = m_N x + \frac{p^2_\perp + m^2}{2\nu z(1-z)} + k(1-\cos\theta) \quad . \tag{49}$$

For a given $q\bar{q}$ configuration $(p_\perp, z)$, and a given (soft) gluon energy k, the angular distribution of the gluon will be given by

$$P(k) \propto \frac{\cos^2\theta (p^x_\perp)^2 + (p^y_\perp)^2}{[1 + A(1-\cos\theta)]^2} \quad , \tag{50}$$

where

$$A = \frac{2\nu z(1-z)}{p^2_\perp + \varepsilon^2} k \quad . \tag{51}$$

In terms of the gluon rapidity

$$\eta_g = \frac{1}{2} \log \frac{1+\cos\theta}{1-\cos\theta} = -\log\tan\frac{\theta}{2} \quad , \tag{52}$$

and of the (slow) quark rapidity η_q given by Eq. (41) we have

$$1 + A(1-\cos\theta) \simeq 1 + \frac{2k}{m_\perp} \frac{e^{\eta_q}}{1+e^{2\eta_g}} \quad . \tag{53}$$

This denominator will suppress the probability (50) of gluon emission unless the gluon rapidity is sufficiently high;

$$2\eta_g \gtrsim \log\left(\frac{2k}{m_\perp}\right) + \eta_q \tag{54}$$

The softest gluons with $k \simeq m_\perp$ thus have rapidities $\eta_g \gtrsim \eta_q/2$. Harder gluons with $k \simeq z\nu$ will be emitted at rapidities between the fast and the slow quark, $\eta_g \gtrsim \eta_q$, outside the rapidity gap to the target.

Thus the gluons associated with the photon Fock state tend to have rapidities in the photon fragmentation region, since this minimizes the off-shellness of the photon wavefunction.

The above argument concerns gluons that are "preformed" in the photon wave function before the target interaction. The two (Coulomb) gluon interactions with the target occur during a very short time interval from the point of view of the photon. Hence, although the projectile system is momentarily a color octet after the first gluon exchange, there is no formation time available for (fast) gluon emission before the second gluon is exchanged. Thus we do not expect that gluons emitted in the short interaction interval can fill more than a limited part of the rapidity gap, close to target rapidities.

We have in this paper neglected higher order contributions where the diffractive scattering occurs off a slow gluon, rather than a quark, in the photon wave function. The amplitude will still factorize as in Eq. (27) into a Fock state amplitude V and a gluon diffractive scattering amplitude W. At lowest order the gluon Fock state amplitude should approximately be given by $V(q\bar{q}g)$ of Eq. (46). The quark configuration will now be a typical one, with $z = \mathcal{O}(1/2)$ and $p_\perp^2 = \mathcal{O}(Q^2)$. The gluon must in this case contribute significantly to ΔE of Eq. (49), having a finite $k_\perp$ in the scaling limit to maintain a constant diffractive (two-gluon exchange) cross section. Just as in our analysis of quark diffractive scattering, this implies $k_z = \mathcal{O}(k_\perp^2/m_N x)$. The probability for such gluon Fock states scales like $1/Q^2$, as can be seen by using Eqs. 48 and 49 in the small θ limit,

$$\alpha_s \frac{p_\perp^2}{\nu^2 z^2 (1-z)^2} \int_0^{\Lambda^2} dk_\perp^2 \int_0^{k_\perp^2/m_N x} \frac{dk_z}{k_z} \frac{1}{(m_N x + k_\perp^2/2k_z)^2} = \mathcal{O}(\alpha_s \frac{\Lambda^2}{Q^2}) \ . \qquad (55)$$

Since the gluon diffractive cross section will be independent of Q^2 due to the finite transverse size of the gluon distribution, we have a scaling contribution to hard diffractive scattering. By including Fock states with multiple gluons we may expect to gradually build up the gluon ladder or "hard Pomeron" [3].

5 Conclusions

In this work we have shown a way to systematically analyze, fully within perturbative QCD, the physical origin and dynamical dependence of rapidity gaps in deep inelastic lepton scattering. Our major simplifying assumption was the use of a heavy quark target so that the physics of the PQCD Pomeron could be directly identified with Coulomb gluon exchange between the heavy target and the constituents of the virtual photon. Color-octet exchange from one or more Coulomb gluons coupled to the target is expected to generate a radiative pattern

in the final state which occupies the entire rapidity interval between the target and virtual photon fragmentation regions. On the other hand, color–singlet exchange arising from two or more Coulomb gluons corresponds to an absence of soft radiation in the central rapidity region.

Our calculation shows explicitly the conservation of impact parameters in DIS at small x [7]. This leads to a very simple factorized structure of the scattering amplitude, with the two–gluon eikonal factor W_2 (Eq. (25)) given by the square of the single gluon factor W_1 (Eq. (15)).

Due to our use of perturbation theory, the explicit expressions we obtained for the scattering amplitudes incorporate general features required by field theory. It is, for example, a well–known feature of QED that single (Coulomb) photon exchange in Bethe–Heitler lepton pair photoproduction gives a cross section that increases logarithmically with photon energy ν,

$$\sigma_{\gamma Z\to \ell^+\ell^- Z} \sim \frac{\alpha(Z\alpha)^2}{m_\ell^2}\, \ell n\, \frac{\nu}{m_\ell} \quad . \tag{56}$$

The logarithm is due to an integration over large impact parameters $R_\perp$, the upper limit being kinematically given by $R_\perp < 1/K_z^{\min} = m_\ell^2/2\nu$. In our approach this logarithm is a direct consequence of the fact that $W_1 \propto r_\perp/R_\perp$ for large target impact parameters $R_\perp$, *cf* Eq. (26). The fact that multiple Coulomb photon exchange does not give logarithmically enhanced contributions [12] then follows directly from Eq. (25), $W_2 \propto W_1^2 \propto r_\perp^2/R_\perp^2$, and its generalizations. This difference in impact parameter dependence shows that the inclusive and diffractive DIS processes are dynamically distinct, and that their ratio cannot be characterized by a single color–dependent constant.

In QED the logarithm of Eq. (56) saturates at $R_\perp = \mathcal{O}(1\ \text{Å})$, where the scattering becomes coherent over the entire electrically neutral atom. In QCD the saturation for gluon exchange will occur at the color confinement radius $R_\perp = \mathcal{O}(1\ \text{fm})$, where perturbative methods cease to apply.

In analyzing the structure of our diffractive cross section (32) we found it important to distinguish between the case of fixed (small) momentum transfer $\mathbf{K}$ to the target, and scattering involving a target momentum transfer that increases with the virtuality Q^2 of the photon.

For small momentum transfers $\mathbf{K}$ we found that only the "aligned jet" region contributes to diffractive scattering in the scaling limit. This region is characterized by one of the quarks taking nearly all of the photon momentum, and by the transverse size $r_\perp$ of the quark pair remaining finite in the scaling limit. Hence multiple gluons can couple to the pair at leading twist. This is in contrast to the "symmetric jet" region where the vanishing size of the pair allows only a single gluon to couple. Since the size of a heavy quark pair is $r_\perp \lesssim \mathcal{O}(1/m)$, two–gluon exhange is similarly suppressed in heavy quark production, leading to a diffractive cross section proportional to $1/m^2$. Analogously, the production of large $p_\perp$ jets at the photon vertex is suppressed by $1/p_\perp^2$ in diffractive scattering.

It will be important to search for these effects experimentally. These features are, however, true only at lowest order, when transverse gluon radiation is neglected.

Most of the HERA data [14] has been selected for low–mass target diffraction, which kinematically allows for a long rapidity gap between the photon and target fragments. It is clearly of interest to study also whether the hardness of the virtual photon can be transmitted to the target fragments in diffractive events [15]. This would not be expected in a model where the scattering occurs via "soft" Pomeron exchange, similar to that observed in hadron scattering at low momentum transfers. In our approach we found, to the contrary, that the contribution from small target impact parameters $R_\perp$ is quite important and only suppressed by powers of the running coupling $\alpha_s(Q^2)$. In inclusive DIS the corresponding subprocess would be classified as $\gamma^* t \to q\bar{q}t$, where t can be any parton (light quark or gluon) of the target. Once $R_\perp = \mathcal{O}(r_\perp)$, the exchange of multiple gluons to the $q\bar{q}$ pair is not power suppressed no matter how small $r_\perp$ is, and the diffractive process can proceed at leading twist. In this large momentum transfer region perturbative calculations are actually the most reliable.

We also considered the modifications brought to the above picture by radiative gluons. Soft gluons emitted in color–singlet exchange processes will mostly occupy the rapidity region between the quarks produced at the photon vertex, thus leaving intact a central rapidity gap extending to the target fragmentation region. At higher orders there are also contributions from photon Fock states where the quark pair is in a transversally compact "symmetric jet" configuration while a soft gluon maintains a finite transverse distance to the quark pair in the scaling limit [4]. The soft gluon can scatter diffractively (through two–gluon exchange), allowing heavy quarks and large $p_\perp$ jets to be produced at the photon vertex at leading twist. These contributions tend to have large diffractive mass, and thus contribute to the region of low $\beta = Q^2/(Q^2 + M^2)$. They are, in fact, the beginning of the gluon ladder which presumably generates the BFKL Pomeron [3]. It should be possible to extend the present calculation in this direction – the more rungs in the ladder that are considered the less important should be our assumption of a heavy quark target.

Acknowledgements

We are grateful for useful discussions with W. Buchmüller and A. Hebecker.

Appendix

Here we wish to collect some useful formulas concerning electroproduction and the virtual photon wave function.

A1. Virtual Photon Factorization.

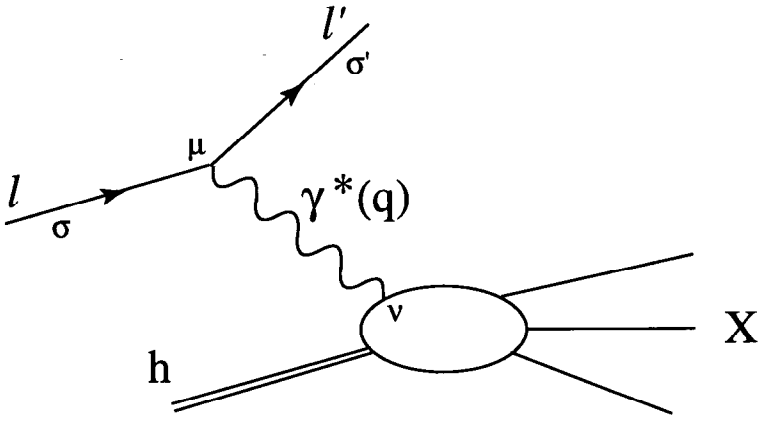

Figure 5: The amplitude for deep inelastic lepton scattering, $\ell + h \to \ell' + X$.

In the notation of Fig. A1, the lepton scattering amplitude is

$$T(\ell h \to \ell' h') = \frac{1}{Q^2}\, j_\ell^\mu (-g_{\mu\nu}) j_h^\nu \quad , \tag{57}$$

where $j_\ell^\mu = e\ \bar{u}_{\sigma'}(\ell')\gamma^\mu u_\sigma(\ell)$ is the lepton current and j_h^ν is the target (hadron) vertex. We choose the target (h) rest frame where the virtual photon momentum is aligned with the z-axis,

$$q = (\nu, \mathbf{0}_\perp, \sqrt{\nu^2 + Q^2}) \quad . \tag{58}$$

Gauge invariance, $q^\mu j_\mu = 0$, implies

$$j^0_{\ell,h} = \frac{q^z}{q^0} j^z_{\ell,h} \quad . \tag{59}$$

Eliminating the $\mu,\ \nu = 0$ components in Eq. (57) we can express the photon exchange in terms of its transverse and longitudinal polarizations,

$$T = \frac{1}{Q^2} \sum_{\lambda=\pm1,0} (-1)^{\lambda+1} \mathbf{j}_\ell \cdot \boldsymbol{\varepsilon}^*(\lambda)\ \boldsymbol{\varepsilon}(\lambda) \cdot \mathbf{j}_h \quad , \tag{60}$$

where

$$\begin{aligned} \boldsymbol{\varepsilon}(\lambda = \pm 1) &= -\frac{1}{\sqrt{2}}(1, \pm i, 0) \quad , \\ \boldsymbol{\varepsilon}(\lambda = 0) &= \frac{Q}{\nu}(0, 0, 1) \quad . \end{aligned} \tag{61}$$

We define the azimuthal angular orientation by fixing the hadronic vertex at $\varphi = 0$, while

$$\ell' = (\nu(1-y)/y, \ell_\perp \cos\varphi, \ell_\perp \sin\varphi, \ell'^z) \quad , \tag{62}$$

where $\nu = y\ell^0$.

The following expressions will be given in the scaling limit,

$$\left\{ \begin{array}{l} Q^2 \to \infty \\ \nu \to \infty \end{array} \right. \quad \text{with} \quad x = \frac{Q^2}{2m_N\nu} \quad \text{fixed}, \tag{63}$$

where m_N is the nucleon mass. We have then

$$\begin{aligned} \ell_\perp &= \ell'_\perp = Q\sqrt{1-y}/y \ , \\ \ell'^z &= \nu(1-y)/y \ . \end{aligned} \tag{64}$$

The spin–averaged square of the scattering amplitude T in Eq. (60) can be written

$$\overline{|T|^2} = \frac{1}{Q^4} \sum_{\lambda,\lambda'} (-1)^{\lambda+\lambda'} L_{\lambda\lambda'} H_{\lambda\lambda'} \ , \tag{65}$$

where

$$L_{\lambda\lambda'} = \frac{1}{2} \sum_{\text{spins}} \mathbf{j}_\ell \cdot \boldsymbol{\varepsilon}^*(\lambda)\ \mathbf{j}^*_\ell \cdot \boldsymbol{\varepsilon}(\lambda') = L^*_{\lambda'\lambda} \ . \tag{66}$$

Explicitly,

$$\begin{aligned} L_{\pm1,\pm1} &= e^2Q^2\left[1+(1-y)^2\right]/y^2 \ , \\ L_{\pm1,\mp1} &= 2e^2Q^2e^{\mp2i\varphi}(1-y)/y^2 \ , \\ L_{\pm1,0} &= -\sqrt{2}e^2Q^2e^{\mp i\varphi}\sqrt{1-y}(2-y)/y^2 \ , \\ L_{0,0} &= 4e^2Q^2(1-y)/y^2 \ . \end{aligned} \tag{67}$$

The hadronic tensor is

$$H_{\lambda'\lambda} = \frac{1}{2} \sum_{\text{spins}} \mathbf{j}^*_h \cdot \boldsymbol{\varepsilon}^*(\lambda')\ \mathbf{j}_h \cdot \boldsymbol{\varepsilon}(\lambda) = H^*_{\lambda\lambda'} = H_{-\lambda',-\lambda} \ , \tag{68}$$

where the last equality applies if we choose H to be real, which is always possible by a choice of frame. With the expressions (68) for $L_{\lambda\lambda'}$ we find for $\overline{|T|^2}$ in Eq. (65),

$$\begin{aligned} \overline{|T|^2} &= \frac{4e^2}{y^2Q^2}\left\{\frac{1}{2}[1+(1-y)^2]\ H_{11} + (1-y)H_{00}\right. \\ &+ \left.(2-y)\sqrt{2(1-y)}\cos\varphi\ \mathrm{Re}(H_{10}) + (1-y)\cos(2\varphi)\ H_{1,-1}\right\} \ , \end{aligned} \tag{69}$$

which is the general expression for the hadronic tensor assuming only single photon exchange between the lepton and hadron vertices (see for example Ref. [17]).

A2. Virtual Photon Wave Function.

The standard covariant expression for the $\gamma \to q\bar{q}$ vertex at lowest order (Fig. A2) is

$$iT_\lambda^{\lambda_1\lambda_2} = \bar{u}_{\lambda_1}(p_1)\left[-iee_q\delta_{AB}(-\boldsymbol{\varepsilon}(\lambda)\cdot\boldsymbol{\gamma})\right]v_{\lambda_2}(p_2)2\pi\delta(E_\gamma - E_1 - E_2) \ , \qquad (70)$$

where $E_\gamma \equiv \nu$ is the (virtual) photon energy, $E_i = \sqrt{\mathbf{p}_i^2 + m^2}$ are the quark energies, A, B the quark colors, and we suppressed the 3–momentum conserving δ–functions. The photon polarization vectors $\boldsymbol{\varepsilon}(\lambda)$ are given in by Eq. (61), and include the longitudinal ($\lambda = 0$) polarization for virtual photons with $q^2 = -Q^2 \neq 0$.

Figure 6: Lowest order diagram describing the $q\bar{q}$ Fock state of the photon.

We shall define the photon wave function $V_\lambda^{\lambda_1\lambda_2}\delta_{AB}$ by Eq. (70) with the replacement

$$2\pi\delta(E_\gamma - E_1 - E_2) \to \int_{-\infty}^{0} dt \exp[-\mathrm{i}t(E_\gamma - E_1 - E_2 + \mathrm{i}\epsilon)] \ , \qquad (71)$$

implying

$$iV_\lambda^{\lambda_1\lambda_2}\delta_{AB} = \frac{-ee_q\delta_{AB}}{E_\gamma - E_1 - E_2 + i\epsilon}\bar{u}_{\lambda_1}(p_1)\boldsymbol{\varepsilon}(\lambda)\cdot\boldsymbol{\gamma}\, v_{\lambda_2}(p_2) \ . \qquad (72)$$

Physically, $V_\lambda^{\lambda_1\lambda_2}$ is the lowest order amplitude for finding a $q\bar{q}$ pair at a given time ($t = 0$), given a bare photon at $t = -\infty$. The time t of the transition $\gamma \to q\bar{q}$ is summed over the interval $-\infty < t < 0$.

The concept of a photon wave function is natural in the scaling limit (63), where the mass Q of the photon is much less than its energy $E_\gamma = \nu$. In this limit, Eq. (72) simplifies to

$$V_\lambda^{\lambda_1\lambda_2}(z, \mathbf{p}_\perp) = -iee_q\frac{2\nu z(1-z)}{p_\perp^2 + \varepsilon^2}\bar{u}_{\lambda_1}(p_1)\boldsymbol{\varepsilon}(\lambda)\cdot\boldsymbol{\gamma}\, v_{\lambda_2}(p_2) \ , \qquad (73)$$

where z is the fraction of the longitudinal momentum carried by the quark,

$$\begin{aligned} \mathbf{p}_1 &= z\mathbf{q} + \mathbf{p}_\perp \ , \qquad (74) \\ \mathbf{p}_2 &= (1-z)\mathbf{q} - \mathbf{p}_\perp \ , \end{aligned}$$

while

$$\varepsilon^2 = m^2 + z(1-z)Q^2 \quad . \tag{75}$$

We shall use the helicity basis for the Dirac spinors,

$$\begin{aligned} u_\lambda(p) &= \frac{\not{p} + m}{\sqrt{E+m}} \begin{pmatrix} \chi_\lambda(p) \\ 0 \end{pmatrix} \quad , \\ v_\lambda(p) &= \frac{-\not{p} + m}{\sqrt{E+m}} \begin{pmatrix} 0 \\ \chi_{-\lambda}(p) \end{pmatrix} \quad , \end{aligned} \tag{76}$$

where the 2-component spinors $\chi_\lambda(p)$ are given in terms of the polar and azimuthal angles θ, φ of $\mathbf{p}$ as

$$\begin{aligned} \chi_{\frac{1}{2}}(p) &= \begin{pmatrix} \cos(\theta/2) \\ e^{i\varphi}\sin(\theta/2) \end{pmatrix} \quad , \\ \chi_{-\frac{1}{2}}(p) &= \begin{pmatrix} -e^{-i\varphi}\sin(\theta/2) \\ \cos(\theta/2) \end{pmatrix} \quad . \end{aligned} \tag{77}$$

In the scaling limit (63) we have

$$\begin{aligned} V^{\lambda_1,\lambda_2}_{\lambda=\pm 1}(z,\mathbf{p}_\perp) &= -iee_q \frac{\nu\sqrt{2z(1-z)}}{p_\perp^2 + \varepsilon^2} \\ \times & \left\{ p_\perp e^{i\lambda\varphi}\delta_{\lambda_1,-\lambda_2}\left[z(\lambda - 2\lambda_2) + (1-z)(\lambda + 2\lambda_2)\right] - 2m\delta_{\lambda,2\lambda_1}\delta_{\lambda_1,\lambda_2}\right\} \quad , \end{aligned} \tag{78}$$

and

$$V^{\lambda_1,\lambda_2}_{\lambda=0}(z,\mathbf{p}_\perp) = -iee_q \frac{4\nu Q[z(1-z)]^{3/2}}{p_\perp^2 + \varepsilon^2} 2\lambda_1 \delta_{\lambda_1,-\lambda_2} \quad . \tag{79}$$

It is useful to express the photon wave function in impact parameter space, through the Fourier transform

$$V^{\lambda_1,\lambda_2}_{\lambda}(z,\mathbf{r}_\perp) = \int \frac{d^2\mathbf{p}_\perp}{(2\pi)^2}\, \mathrm{e}^{\mathrm{i}\mathbf{r}_\perp\cdot\mathbf{p}_\perp}\, V^{\lambda_1,\lambda_2}_{\lambda}(z,\mathbf{p}_\perp) \quad . \tag{80}$$

The integral in Eq. (80) can be explicitly performed, for the photon wave functions in Eqs. (78) and (79), as well as for the other amplitudes discussed in the text, by using the identity

$$\int_0^\infty du \frac{u^{n+1}}{u^2 + a^2} J_n(u) = a^n K_n(a) \quad , \tag{81}$$

where J_n and K_n are Bessel functions, and the identity applies for $n < 3/2$. The results can be written as

$$\begin{aligned} V^{\lambda_1,\lambda_2}_{\lambda=\pm 1}(z,\mathbf{r}_\perp) &= \frac{-\mathrm{i}}{2\pi}\, ee_q\, \nu\sqrt{2z(1-z)}\, \{-2m\ \delta_{\lambda,2\lambda_1}\ \delta_{\lambda_1,\lambda_2} K_0(\varepsilon r_\perp) \\ &+ \mathrm{i}\, \mathrm{e}^{\mathrm{i}\lambda\varphi_r}\delta_{\lambda_1,-\lambda_2}\left[z(\lambda - 2\lambda_2) + (1-z)(\lambda + 2\lambda_2)\right]\varepsilon K_1(\varepsilon r_\perp)\Big\} \\ V^{\lambda_1,\lambda_2}_{\lambda=0}(z,\mathbf{r}_\perp) &= \frac{-\mathrm{i}}{2\pi}\, ee_q\, \nu\, Q\, 4\left[z(1-z)\right]^{3/2} 2\lambda_1\ \delta_{\lambda_1,-\lambda_2}\ K_0(\varepsilon r_\perp) \quad , \end{aligned} \tag{82}$$

where φ_r is the azimuthal angle of $\mathbf{r}_\perp$.

As shown in Section 2, the scattering amplitudes with one and two gluon exchanges off a massive target are, in the small x limit, proportional to the photon wave functions in Eq. (82).

References

[1] J. Bjorken, AIP Conference Proceedings No. 6, Particles and Fields Subseries No. 2, Ed. M. Bander, G. Shaw and D. Wong (AIP, New York, 1972); J. D. Bjorken and J. Kogut, Phys. Rev. D **8**, 1341 (1973); J. D. Bjorken, preprint SLAC–PUB–7096 (1996), hep-ph/9601363.

[2] G. Ingelman and P. Schlein, Phys. Lett. **B152**, 256 (1985); A. Donnachie and P. V. Landshoff, Phys. Lett. **B191**, 309 (1987); K. Golec–Biernat and J. Kwiecinski, Phys. Lett. **B353**, 329 (1995), hep-ph/9504230; E. L. Berger, J. C. Collins, D. E. Soper and G. Sterman, Nucl. Phys. **286**, 704 (1987).

[3] A. H. Mueller, Nucl. Phys. **B335**, 115 (1990); M. G. Ryskin, Sov. J. Nucl. Phys. **52**, 529 (1990); N. N. Nikolaev and B. G. Zakharov, Z. Phys. **C53**, 331 (1992). J. Bartels, H. Lotter and M. Wusthoff, Z. Phys. **C68**, 121 (1995), hep-ph/9501314, and Phys. Lett. **B379**, 239 (1996), Erratum in Phys. Lett. **B382**, 449 (1996), hep-ph/9602363; J. Bartels and M. Wusthoff, J. Phys. **G22**, 929 (1996).

[4] W. Buchmüller and A. Hebecker, Phys. Lett. **B355**, 573 (1995), hep-ph/9504374; A. Edin, G. Ingelman and J. Rathsman, Phys. Lett. **B366**, 371 (1996), hep-ph/9508386; W. Buchmüller, M. F. McDermott and A. Hebecker, DESY 96–126, hep-ph/9607290.

[5] L. Frankfurt and M. Strikman, proceedings of the Workshop on Deep Inelastic Scattering and QCD (DIS 95), Paris, France, 24–28 Apr 1995, hep-ph/9510291; A. Berera and D. E. Soper, Phys. Rev. D **53**, 6162 (1996), hep-ph/9509239.

[6] V. Del Duca, S. J. Brodsky and P. Hoyer, Phys. Rev. D **46**, 931 (1992).

[7] N. N. Nikolaev and B. G. Zakharov, Z. Phys. **C49**, 607 (1991).

[8] B. Kopeliovich and B. Povh, MPI H–V28–1996, To appear in Proceedings of the Workshop on Future Physics at HERA, DESY 1995–96, hep-ph/9607035.

[9] S. J. Brodsky, A. Hebecker, and E. Quack, SLAC–PUB–7257, (1996), hep-ph/9609384.

[10] H. N. Chehime and D. Zeppenfeld, preprint MAD/PH/814 hep-ph/9401244.

[11] Yu. I. Azimov, Yu. I. Dokshitzer, V. A. Khoze and S. I. Troyan, Phys. Lett. **165B**, 147 (1985).

[12] H. A. Bethe and L. C. Maximon, Phys. Rev. **93**, 768 (1954); H. Davies, H. A. Bethe and L. C. Maximon, Phys. Rev. **93**, 788 (1954).

[13] M. Genovese, N. N. Nikolaev and B. G. Zakharov, Phys. Lett. **B378**, 347 (1996), hep-ph/9603285; E. M. Levin, A. D. Martin, M. G. Ryskin and T. Teubner, preprint DTP/96/50, hep-ph/9606443.

[14] H1 Collaboration, T. Ahmed *et al.*, Phys. Lett. **B348**, 681 (1995), hep-ex/9503005; ZEUS Collaboration, M. Derrick *et al.*, Z. Phys. **C68**, 569 (1995), hep-ex/9505010.

[15] ZEUS Collaboration, M. Derrick *et al.*, Phys. Lett. **B369**, 55 (1996), hep-ex/9510012.

[16] S. J. Brodsky, L. Frankfurt , J. F. Gunion, A. H. Mueller, M. Strikman, Phys. Rev. **D50**, 3134 (1994), hep-ph/9402283.

[17] Ch. Rumpf, G. Kramer and J. Willrodt, *Z. Phys.* **C 7** (1981) p. 337.